Journal of Paleontological Techniques

Number 18 May 2017

COUPLING FOCUS STACKING WITH PHOTOGRAMMETRY TO ILLUSTRATE SMALL FOSSIL TEETH

Michael Santella[1] & Andrew R. C. Milner[1]

1 - St. George Dinosaur Discovery Site at Johnson Farm, St. George, Utah, USA

Emails: mlsantella@gmail.com (MS), arcmilner@gmail.com (AM)

ABSTRACT

A macrophotography technique coupled with focus stacking was used to produce source images for photogrammetry of two isolated fossil teeth from the Lower Jurassic Kayenta Formation of southwest Utah. The crown heights of the teeth are approximately 4 mm and 9 mm. The macrophotography was conducted using a Canon digital camera body with a 24-megapixel APS-C sensor. The camera body was attached to a Canon MP-E 65mm lens. A Cognisys focusing rail coupled to a rotation stage was used to manipulate specimens for photography. Focus stacking with Helicon Focus 6 software was used to produce completely focused images for input to Agisoft Photoscan photogrammetry software. The scaled three-dimensional representations created by photogrammetry are available at https://figshare.com/s/d205f5bee8cb2767f902 for specimen UMNH VP 25852 and https://figshare.com/s/af8b4e74db21606a91bd, for specimen UMNH VP 25853. Judging by appearances, retention in the three-dimensional models of shape and surface details from the two-dimensional input images was excellent. A stereo lithography file was also exported for UMNH VP 25852 model, and it was used to produce a 3D-printed model. Regarding identification of the teeth, specimen UMNH VP 25852 has features associated with small theropod dinosaurs. Specimen UMNH VP 25853 has features associated with ornithischian dinosaurs. However, without reference to skeletal remains neither tooth could be unambiguously associated with a specific taxon.

RESUMO [in Portuguese]

Uma técnica de macrofotografia associada ao empilhamento de focagem foi usada para produzir imagens de origem para fotogrametria de dois dentes fósseis isolados, da Formação Kayenta do Jurássico inferior do sudoeste de Utah. A altura das coroas dos dentes é de aproximadamente 4 mm e 9 mm. A macrofotografia foi conduzida usando um corpo de câmara digital Canon, com um sensor APS-C de 24 megapixels. O corpo da câmara foi acoplado a uma lente Canon MP-E 65mm. Um Cognisys com carreto de focagem acoplado a um mecanismo de rotação foi usado para manipular os espécimes para a fotografia. O empilhamento de imagens com diferentes focagem foi realizado com o software Helicon Focus 6 para produção de imagens completamente focadas para serem inseridas no software de fotogrametria Agisoft Photoscan. As representações tridimensionais escalonadas criadas pela fotogrametria estão disponíveis em https://figshare.com/s/d205f5bee8cb2767f902 para o espécime UMNH VP 25852 e https://figshare.com/s/af8b4e74db21606a91bd, para o espécime UMNH VP 25853. Ao que parece, a retenção nos modelos tridimensionais dos detalhes da forma e da superfície das imagens bidimensionais da entrada foi excelente. Um arquivo de litografia estéreo também foi exportado para o modelo UMNH VP 25852, e foi usado para produzir um modelo impresso em 3D. Quanto à identificação dos dentes, o espécime UMNH VP 25852 tem características associadas a pequenos dinossauros terópodes. O espécime UMNH VP 25853 tem características associadas com dinossauros ornitisquios. No entanto, sem associação a um esqueleto permanece ambos os dentes não podem ser inequivocamente associados com um taxon específico.

How to cite this paper: Santella, M. and Milner, A.R.C. (2017). Coupling focus stacking with photogrammetry to illustrate small fossil teeth. Journal of Paleontological Techniques, 18:1-17.

INTRODUCTION

Numerous small fossil teeth from vertebrates were collected during a paleontological resource surface survey in southwest Utah. The major dimension of most of the teeth is less than 12 mm, and this makes detailed examination of the teeth impossible without the aid of magnification. One method for facilitating examination of the teeth, and for sharing details of their shapes and surface features is photogrammetry. Photogrammetry is becoming increasingly valuable for documenting and archiving fossils (Breithaupt et al., 2004; Matthews, 2008; Falkingham, 2012; Mallison and Wings, 2014; Matthews et al., 2016). For instance, the ability to use photogrammetry on small, centimeter-scale specimens was demonstrated (Falkingham, 2012), but its application to specimens too small to be examined in detail without the aid of magnification is not common. This is due in part to complexities associated with photographing small specimens in a way that is compatible with further processing for photogrammetry.

A significant challenge in applying photogrammetry to small specimens is managing the relationship between magnification and depth of field in the source images. Photogrammetry can only reasonably reproduce details that are clearly visible in the images input for analysis. Consequently, getting photogrammetry models of small specimens with good fidelity of important features requires that they be photographed at higher magnifications than those commonly used in conventional photography. However, a by-product of increased magnification is reduced depth of field so that individual images of magnified subjects that are not flat may not be completely in-focus. This can be problematic for acceptable photogrammetry processing. A specific challenge, therefore, for using photogrammetry for small, contoured specimens like teeth is being able to produce suitably magnified images that are fully focused.

This work outlines an approach being used to apply photogrammetry for documenting, archiving, and sharing information about small, vertebrate fossil teeth. The general approach draws from work being done on modern insect specimens (Nguyen et al., 2014), and from various sources of information on applied photogrammetry available on the internet (Cognysis-Inc.com; Porter et al., 2016; Minnesota Anthropology). The details of the photography set-up and the processing needed to prepare images of the teeth for photogrammetry are presented. The ability to capture and magnify the shape and surface details of small fossil teeth are demonstrated with two specific examples of isolated specimens collected from the Silty Facies of the Kayenta Formation in southwest Utah.

MATERIALS AND METHODS

Photography set-up

Sharply-focused images of evenly exposed subjects are the essential input requirement for photogrammetry (Matthews, 2008; Mallison and Wings, 2014; Nguyen et al., 2014; Matthews et al., 2016). All the images for this work were recorded using a Canon T6s digital camera body which has an APS-C sensor size of 22.3 mm x 14.9 mm with a total of 24.2 megapixels (USA.Canon.com, eos). The small sizes of the fossil teeth dictated that macrophotography techniques were needed to capture relevant surface details. This was accomplished by attaching a Canon MP-E 65mm lens to the camera body. This manual-focus lens is specifically designed for macrophotography and it is capable of magnifications of 1-5X (USA.Canon.com, mpe). The working distance range for the lens is limited to approximately 40-100 mm.

The general set-up for the photography followed recommendations outlined by (Nguyen et al., 2014), and illustrated on the Cognisys Inc. web site at https://www.cognisys-inc.com/how-to/stackshot3x/virtual-objects.php The camera was mounted to a focusing rail that was attached to a tripod while the specimens were rotated through 360°. The motions of both the focusing rail and the rotation stage were automatically adjusted with a StackShot 3X controller to produce the desired focus conditions and photographic coverage of specimens. Specimens were fixed onto the heads of mounting pins with small dabs of museum wax (Ready America, Inc., Quake Hold!™) and manually centered about the axes of the pin shafts. The pin shafts were held in a pin vise that was machined so that it threaded into the center of the rotation stage (Cognisys, Inc., ShackShot 3X). The result of this arrangement is illustrated in Figure 1 for

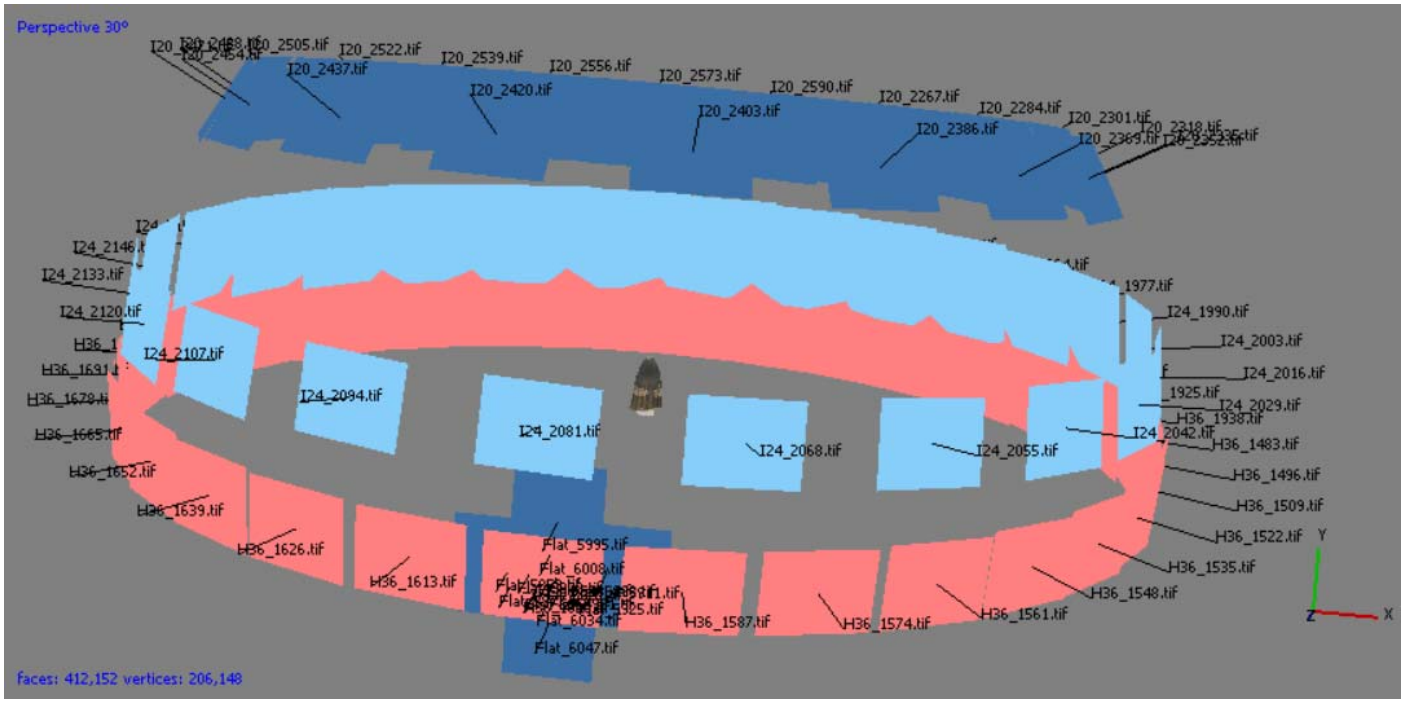

Figure 1: Illustration of the 94 camera positions used to photograph specimen UMNH VP 25852 for photogrammetry. Eighty images were used for circuits around the specimen; 14 images were used for scaling.

specimen UMNH VP 25852. It was photographed at 10° rotational intervals with the camera held horizontally, 15° rotational intervals at an inclination angle of 10°, and 18° rotational intervals with the camera inclined 30° relative to horizontal. This resulted in a total of 80 individual camera positions encircling the specimen in three circuits. Also, shown in the lower left quadrant of Figure 1, is the group of 14 images recorded for scaling. The images for scaling were recorded with the tooth held stationary while the camera was repositioned as recommended by Matthews (2008) and by Matthews et al. (2016). Reference scales with divisions of 1 mm were also captured in these images. A similar strategy was also used for photographing UMNH VP 25853.

All images were recorded in the RAW file format with the camera in the full manual mode using an f/16 aperture setting and exposure times of 0.8 s for specimen UMNH VP 25852 and 0.3 s for specimen UMNH VP 25853. Continuous lighting was provided by two 25-W, 2,000-lumen LED work lights (Snap-on model no. 871356U) set on either side of the camera lens. No flash was used. An important addition to the camera lens was a circular polarizing filter which minimized specular reflections from the teeth surfaces. All the photographs were taken against a turquoise background to aid in subsequent image processing.

Depth of field considerations

Multiple exposures were required at each of the camera positions because fully focused images were not possible with a single exposure due to the contoured shapes of the teeth and the way high magnifications and small working distances limit depth of field. A limited amount of data is available for the variation of depth of field with magnification (USA.Canon.com, mpe). However, Canon data can be reproduced with a standard optical formula (Larmore, 1965) for relating depth of field, *DOF*, to lens focal length, *f*, lens f-number, *N*, magnification, *m*, and circle of confusion value, *c* = 0.035 mm:

$$DOF = \frac{2f(m+1)/m}{fm/Nc - Nc/fm}$$

For a given lens, both the circle of confusion value and the focal length are constants.

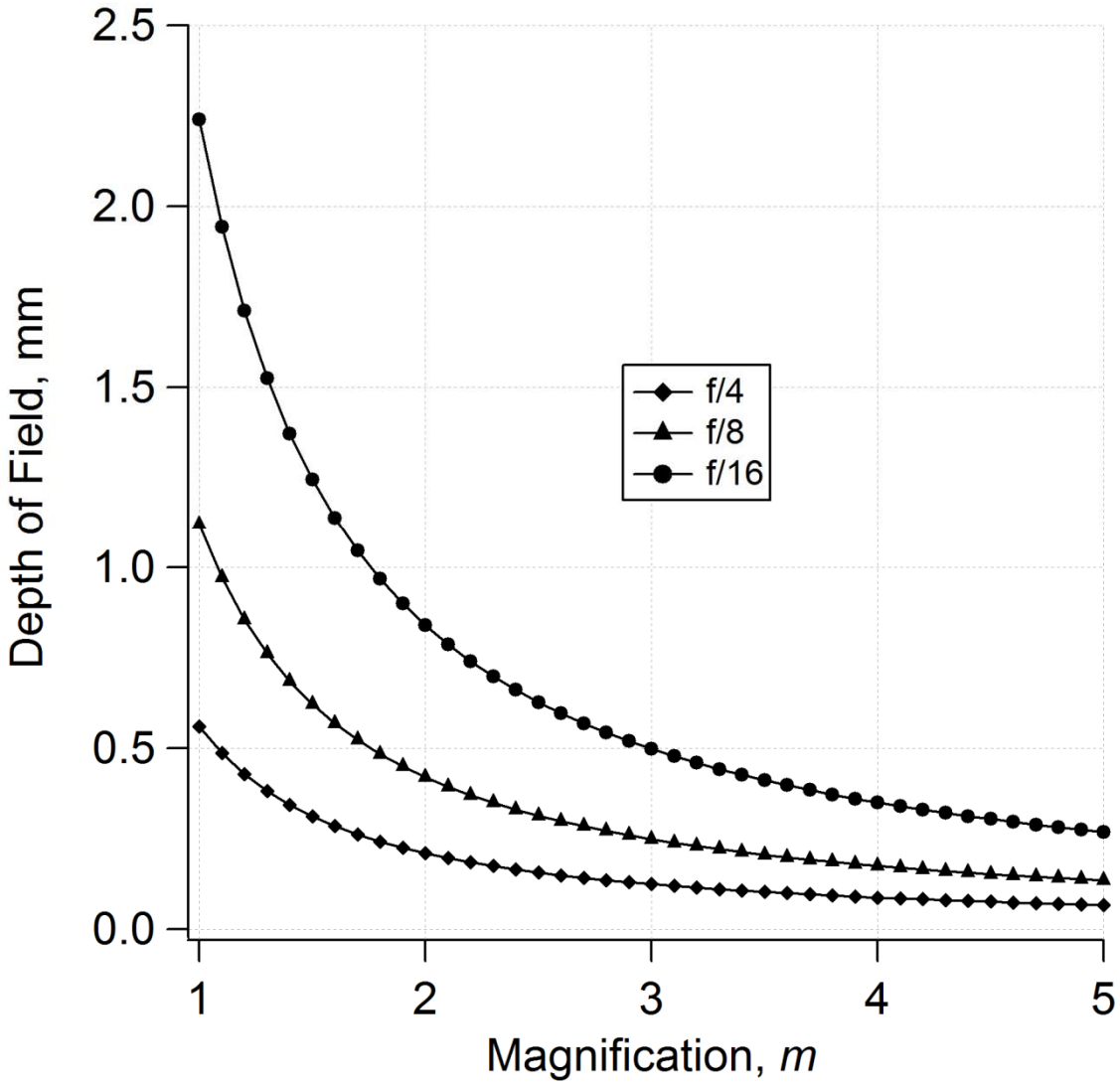

Figure 2: Variation of Depth of Field, DOF, with magnification, m, for a Canon MP-E 65 mm lens.

Consequently, for a fixed f-number, this equation describes the variation of *DOF* with magnification needed to determine the linear intervals used to control the focusing rail for photographing the teeth. The variation of *DOF* with magnification is plotted in Figure 2 which clearly shows *DOF* increases with lens f-number and decreases rapidly with increasing magnification setting.

The photographs were taken with the camera in the portrait orientation so that the long axes of the teeth corresponded to the 22.3 mm sensor dimension. The magnification setting of the lens was then adjusted so that the tooth nearly filled the image frame during a 360° rotation. The magnification values used to estimate *DOF* values were then approximated by measuring the lens position on the lens barrel. This was possible because the integer magnification values are marked on the lens barrel and the interval between the marks is 10 mm. Specimen UMNH VP 25852 was photographed at a magnification of about 2.1X; specimen UMNH VP 25853 used a magnification of about 2.9X. These magnifications corresponded to calculated DOF values, respectively, of 0.787 mm and 0.519 mm. Those were then further reduced to 0.500 mm and 0.300 mm for additional factors of safety in the focusing accuracy.

Once the *DOF* values were established it was then possible to set the focusing conditions at each camera position. For example, at each of the 80 camera positions used to construct the photogrammetric model of Specimen UMNH VP 25852 the focusing rail automatically translated

the camera linearly at intervals of 0.500 mm. The total translation length, which determined the number of focusing intervals at each angle of inclination, was manually set to capture images from the point where in-focused regions were first detected to the point where they were no longer detected.

Archeological artifacts are successfully modeled using inclination angles of up to about 60° at increments of about 20° to horizontal (Porter et al., 2016). Experience with the fossil teeth indicated that inclination angles of no more than about 30° would result in models with acceptable levels of detail even at the tooth apices. Presumably, this was due to the generally conical shapes of the teeth. To record the circuit images for Specimen UMNH VP 25852, first, at the horizontal camera inclination, 13 images were recorded at each of 36 positions using successive 10° rotation intervals. Next, 13 images were recorded at each of 24 successive 15° intervals at the inclination angle of 10°. Finally, 17 images were recorded at each of 20 successive 18° rotational intervals at an inclination angle of 30°. For scaling, 14 camera positions were used with 13 exposures at each position. This resulted in a total of 1,302 individual exposures: (36 x 13) + (24 x 13) + (20 x 17) + (14 x 13). Specimen UMNH VP 25853 was modeled using circuits of only 36 camera positions with 10 images/position at the horizontal inclination, and 24 positions with 11 images/position at an inclination of about 25°. An additional 9 camera positions using 8 individual exposures at each position were used for scaling. The total number of individual exposures for this tooth were (36 x 10) + (24 x 11) + (9 x 8) = 696.

Image processing

The next step in preparing images for photogrammetry consisted of reducing the multiple images to a single image for each camera position. This was done using Helicon Focus Pro software (Version 6.6, Helicon Soft Ltd., www.heliconsoft.com) which automatically compiled the in-focus regions of each image for a particular camera position into a single composite image in which the entire tooth was focused. The sum of 1,302 individual images for Specimen UMNH VP 25852 was subsequently reduced to 94 focus-stacked input images. Similarly, the 696 individual images for UMNH VP 25853 were reduced by focus stacking to 69 input images.

Of the three methods that are available for focus stacking in the Helicon Focus 6 software the one that gave the best retention of surface details, judging by visual appearance, was the procedure designated as Method C. Each focus-stacked image was finally rendered to a file size of about 15 MB and saved in the TIFF file format with LZW compression.

Next, only the focus-stacked circuit images were masked in Photoshop (Porter et al., 2016; Minnesota Anthropology) to block out the background in each image. Images used for scaling were not masked. Finally, the circuit and the scaling focus-stacked, TIFF-format image files where then imported for analysis into Agisoft Photoscan Professional software (Version 1.2.4, Agisoft LLC, www.agisoft.com).

The processing conditions used for the photogrammetry modeling are summarized in Table 1. For both specimens, processing proceeded by first aligning the images used for scaling, optimizing those parts of the models, and applying scale markers to the results (Matthews, 2008; Matthews et al., 2016). In secondary operations, the circuit images were independently aligned all together. Subsequently, the scaling results and the circuit results were aligned and merged together. Finally, these merged results were realigned. The realigned sparse clouds for both specimens were then edited to remove poorly matched and spurious points using the Gradual Selection features in Photoscan. Iterations of the Reconstruction Uncertainty, the Projection Accuracy and the Reprojection Error criteria were used to successively delete about 5-10% of the sparse cloud points followed by the Optimization procedure. This was continued until a Reprojection Error value near 0.3 pixel was achieved. During optimization, care was taken to avoid eliminating images from the final analysis by deleting too many of their associated projections. After the sparse point clouds were optimized and scaling was applied, processing continued by generating dense point clouds, meshing, and applying surface textures. This general process resulted in scaled three-dimensional models with excellent retention of shape and surface details from the two-dimensional input images.

Table 1: Photogrammetry processing summaries

	UMNH VP 25852	**UMNH VP 25853**
Property	**Value**	**Value**
General		
Cameras	94	69
Aligned cameras	94	69
Markers	6	4
Scale bars	3	2
Point Cloud		
Points	31,477 of 91,404	42,633 of 115,775
RMS reprojection error	0.110376 (0.270264 pix)	0.112661 (0.250166 pix)
Max reprojection error	0.331705 (1.30757 pix)	0.305099 (1.89768 pix)
Mean key point size	2.39477 pix	2.03514 pix
Effective overlap	3.36346	2.96269
Alignment parameters		
Accuracy	High	High
Pair preselection	Disabled	Disabled
Key point limit	60,000	60,000
Tie point limit	0	0
Constrain by mask	Yes	Yes
Optimization parameters	f, b1, b2, cx, cy, k1-k4, p1,	f, b1, b2, cx, cy, k1-k4, p1,
Dense point cloud		
Points	1,308,588	921,050
Reconstruction		
Quality	High	High
Depth filtering	Aggressive	Aggresive
Model		
Faces	412,152	500,000
Vertices	206,148	250,091
Texture	4,096 x 4,096	4,096 x 4,096
Reconstruction		
Surface type	Arbitrary	Arbitrary
Source data	Dense	Dense
Interpolation	Enabled	Enabled
Quality	High	High
Depth filtering	Aggressive	Aggressive
Face count	500,000	500,000
Texture parameters		
Mapping mode	Generic	Generic
Blending mode	Mosaic	Mosaic
Texture size	4,096 x 4,096	4,096 x 4,096

The 3D models developed by photogrammetry were finally exported in the PDF, OBJ, and STL file formats. The PDF format creates embedded, rotatable 3D objects in the files which are viewable on any computer system using version 7 or later of the free software, Adobe Acrobat Reader (https://get.adobe.com/reader/). If difficulties are encountered in viewing the 3D models embedded in these PDF files, then either Adobe Acrobat Reader should be updated or a different PDF viewing program should be tried. The OBJ file format is an open-source, universal format for representing three-dimensional geometry. The STL file format is another relatively common format for representing the geometry of three-dimensional objects. It is widely used for rapid prototyping, 3D printing and computer-aided manufacturing. Both OBJ and STL files can be combined with surface texture information to map actual colors onto three-dimensional geometry.

All the image processing, including the photogrammetry, was done using a Lenovo laptop computer with an Intel® Core™ i7-4700HQ CPU, 16 GB of RAM, and the 64-bit Windows 10 operating system.

RESULTS

To the extent possible, the features of these two teeth are described using a combination of terminology recommendations (Smith and Dodson, 2003; Hendrickx et al., 2015).

Specimen UMNH VP 25852

The overall shape and appearance of this crown is shown in Figure 3. It is conical and somewhat symmetrical when viewed in either a mesiodistal or labiolingual direction as shown in Figure 4, but it is compressed in the labiolingual direction. At this point, as this is an isolated tooth with no root and relatively symmetric features, the assignment of specific orientations in both Figure 3 and Figure 4 was a convenience for the sake of discussion. The exposure of the tooth interior shown on the left image in Figure 3 is possible evidence of a resorption pit which would support the assignment of orientations, but this interpretation could not be unambiguously confirmed. The crown height is approximately 9.1 mm; the crown base length is approximately 5.3 mm.

Figure 3: Images showing overall appearance of specimen UMNH VP 25852, hypothetical lingual view (left), and hypothetical labial view (right).

Figure 4: Focus-stacked images showing details, from left to right, of specimen UMNH VP 25852. Left to right: hypothetical mesial view, labial view, distal view, lingual view.

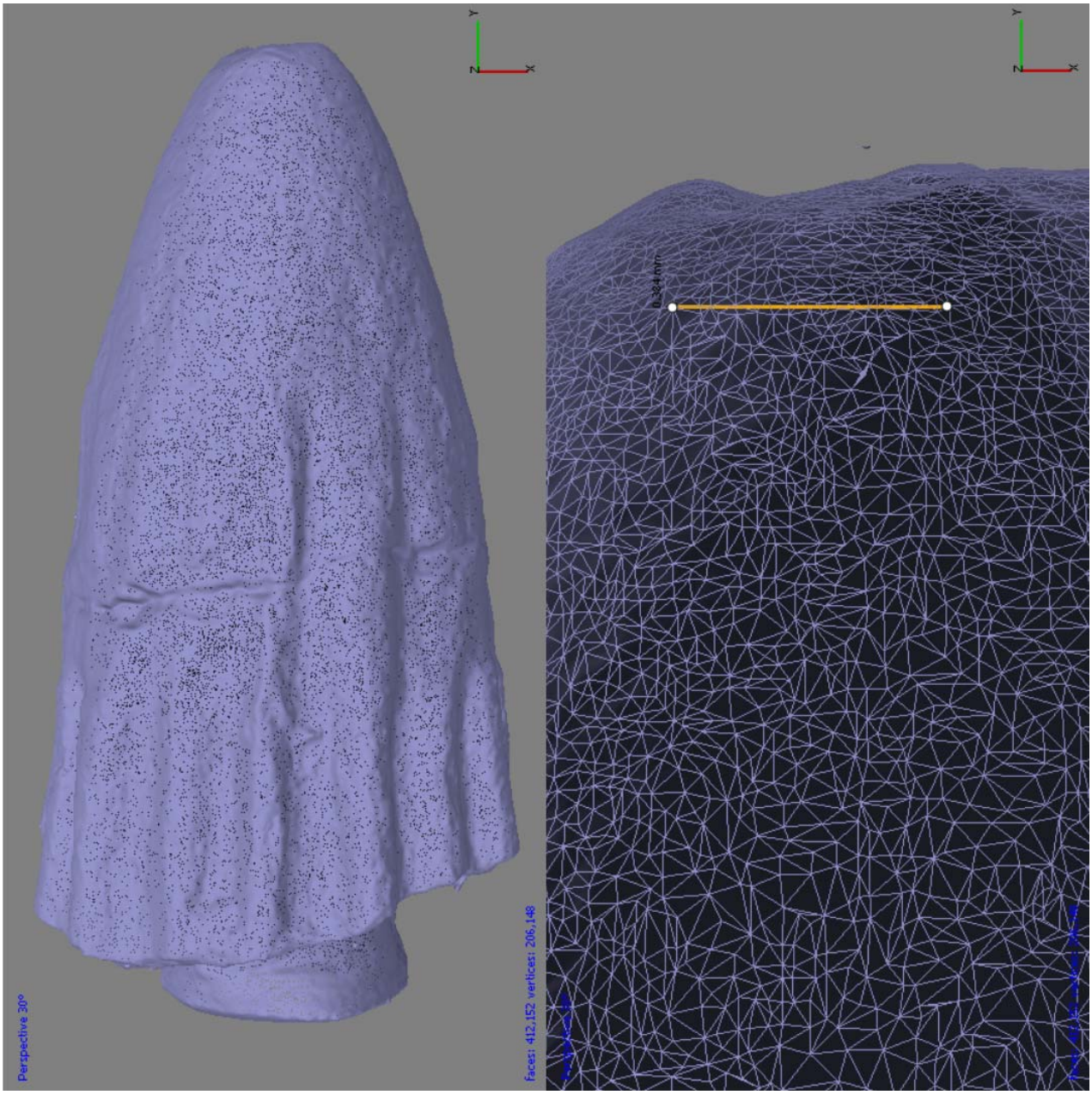

Figure 5: Wireframe model of UMNH VP 25852 showing the entire tooth (left) and a magnified view highlighting the mesh (right). Scale bar = 0.38 mm.

As shown in Figure 3, there are a total of 17 prominent flutes around the crown that extend from about 3 mm below its apex to the margin of the apparent cervix. The flutes are relatively deep and appear to increase slightly in depth as they approach the cervix. The flute-free region below the crown apex also contains a series of transverse undulations. The morphology of the enamel surface is consistent with a braided textured of small ridges oriented apicobasally, (Figure 4). This texture is apparent even within the fluted regions. Also, there is an unserrated carina on both the putative mesial and distal margins. In both cases, the carinae appear to be split. Damage is also apparent on the crown apex and just below the crown along the mesial margin.

An image of the meshed model output from Photoscan is shown in Figure 5 with the entire scaled model on the left and a magnified view of the mesh on the right. The model consisted of 412,152 faces with 206,148 vertices.

Specimen UMNH VP 25853

The overall shape and appearance of this crown is shown as Figure 6. The shape is spatulate in the mesiodistal orientation. The root is no longer attached to the crown but there is a clear expansion of the crown above the cervix. The distal margin is slightly recurved. The crown is compressed in the labiolingual direction (Figure 7), with the lingual surface being convex relative to the apicobasal axis and the lingual side being concave. The radius of curvature is smaller on the lingual side contributing to the observed thickening above the cervix. The crown height is about 4 mm; the crown base length is about 3 mm.

Figure 6: Specimen UMNH VP 25853, lingual view (left), and labial view (right).

Figure 7: Focus-stacked images showing details, from left to right, of specimen UMNH VP 25853: mesial view, labial view, distal view, lingual view.

Flutes are also prominent features on this tooth with the labial side having 7 and the lingual side having 11. On both sides the flutes extend nearly to the apex. A braided surface texture occurs on the enamel surface and it is superimposed on the flutes on both the labial and lingual sides. The appearance of the carinae suggests denticles were present on both, but clearly formed ones are evident only slightly above the cervix. It appears that the size range of the denticles was 0.1-0.2 mm, and that they were oriented 45° or more to the mesial and distal margins. There is visible damage to both the labial surface just above the cervix and to the distal margin just above that location, (Figure 7). The location of the damage suggests it could be due to occlusion with opposing teeth, but this cannot be firmly established.

The mesh for the model of this specimen is shown as Figure 8, with the entire scaled model on the left and a magnified view of the mesh on the right. The model consisted of 500,000 faces with 250,091 vertices.

File sets for viewing both specimens are available for downloading with the internet links: https://figshare.com/s/d205f5bee8cb2767f902, for UMNH VP 25852, and https://figshare.com/s/af8b4e74db21606a91bd, for UMNH VP 25853. Each file set contains three versions of the modeled specimen: (1) a 3D PDF that can be manipulated for viewing from arbitrary perspectives; (2) a short animation in which the specimen rotates 360 degrees; and, (3) the three files resulting from exporting from Photoscan to the OBJ file format. These last three files consist of the 3-dimensional geometry, the texture image, and material data.

Resolution/Sharpness

The ability of the focus stacking and photogrammetry to capture and maintain details is illustrated using images of specimen UMNH VP 25853 in Figure 9. The left image is 1 of 10 recorded at this position which were subsequently combined into the composite, focus-stacked image of Figure 9 (center). The dashed box in the left image highlights the region that is most clearly focused, and the left most of edge of the tooth is clearly out of focus in this image. Comparison with the center image shows that focus stacking created an entirely focused image. The image of Figure 9 (right) is a screen-capture from the exported PDF file of the photogrammetry model with the tooth positioned in the approximate orientation shown in the left and center images. Inspection of this series of images indicates that the loss of spatial resolution and sharpness due to focus stacking and photogrammetry is negligible compared to original images. Spatial resolution was assessed using the procedures and test chart of (ISO 12233, 2000). For both specimens, spatial resolution was estimated at 9 µm.

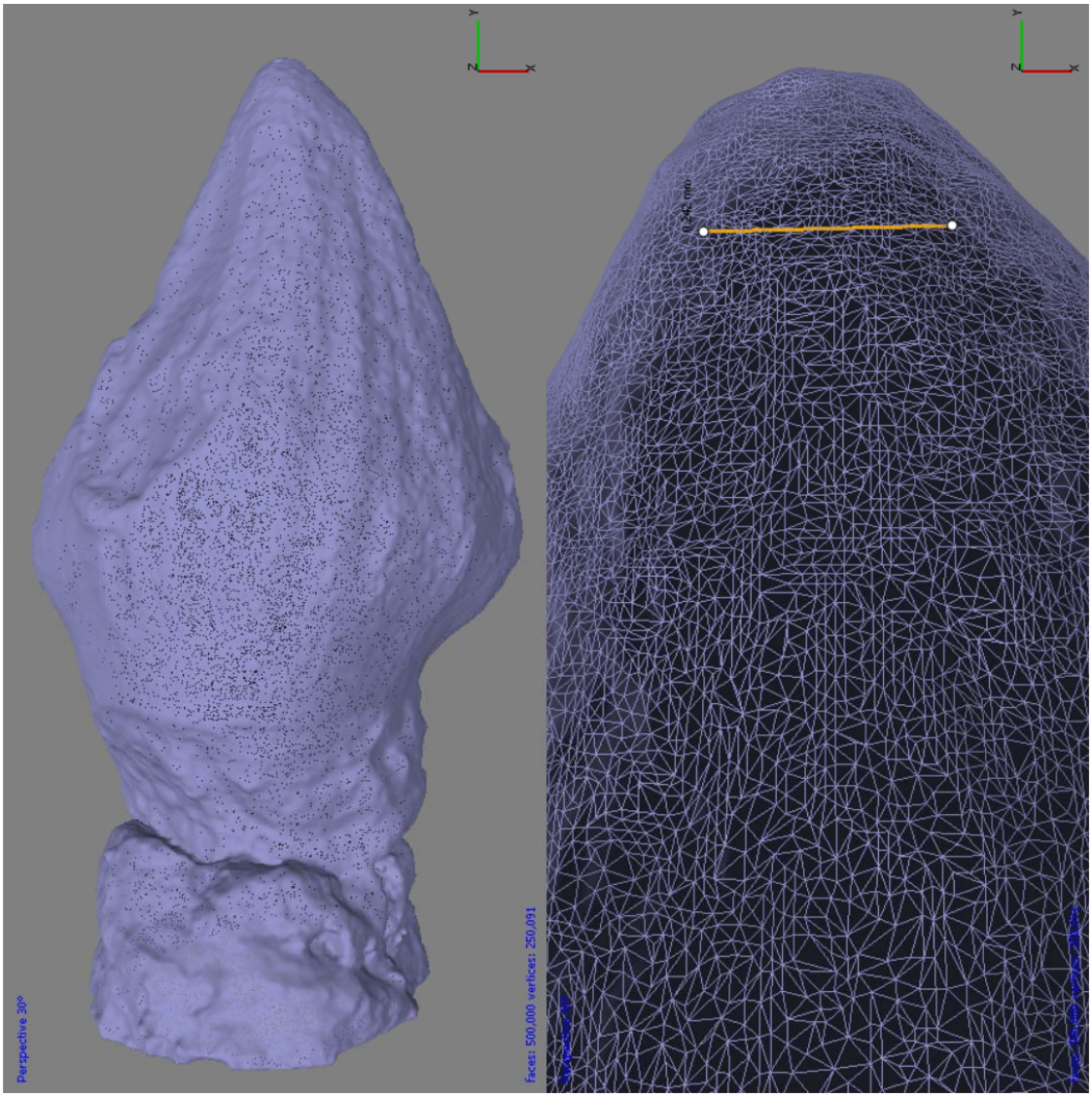

Figure 8: Wireframe model of UMNH VP 25853 showing the entire tooth (left) and a magnified view highlighting the mesh (right). Scale bar = 0.24 mm.

Figure 9: Illustration of resolution showing on the left, one photo from a series used for focus stacking with the in-focus region approximately outlined by the dotted box; the result of focus stacking the same series of images (center); and, a screen-capture image from the associated photogrammetry model (right).

DISCUSSION

Photography/Photogrammetry

Like what was shown for insect collections (Nguyen et al., 2014), this work suggests that photogrammetry coupled with macro-photography techniques has considerable potential benefits for recording, displaying, and sharing information about small fossils. Perhaps more importantly, it provides a useful and convenient means of examining their fine-scale details without additional handling of the specimens. Figure 7 and Figure 9 of UMNH VP 25853 illustrates a disadvantage of frequent handling. As the various processes to produce the photogrammetry models were being developed, this tooth, as well as specimen UMNH VP 25852, was frequently handled. This contrasts with the more typical situation in which specimens would remain relatively untouched after preparation and mounting. Not all the presented images for either tooth were recorded in a single session. Both teeth were remounted, adjusted in position, and photographed multiple times. When the images of Figure 9 were recorded, specimen UMNH VP 25853 was attached to a base of sedimentary rock, the top edge of which is visible near the bottom of these images below the cervix of the tooth. In a subsequent photography session, as this tooth was being repositioned, it detached from its sedimentary base. In this case, the tooth remained intact, but this relatively inconsequential damage still highlights the careful handling required for small and potentially fragile specimens.

Two additional points are illustrated by Figure 9. The first is that although images were subjected to a focus-stacking procedure, then converted from RAW to TIFF file format, and finally processed by Agisoft Photoscan, the visual sharpness and spatial resolution of the results are comparable to the original RAW images. The second point relates to processing of the image files that are shown in the left and center images of Figure 9. Clearly, the focus-stacked image in the center has certain photographic adjustments made to increase the vibrance and saturation of color, for instance. These adjustments were not intentional. Instead, they were made automatically during the focus stacking procedure. The point of mentioning this is that there are default settings embedded in both Photoshop and Helicon Focus 6 that may modify images without an explicit request to do so. For this set of experiments, unrequested adjustments did not create any problems, but, for some situations, they may be undesirable. Further experience with the software should enable better control of these image adjustments.

With the camera body and lens used for this work, simple optics calculations indicate that further increase of spatial resolution is possible. For example, the pixel pitch for this APS-C sensor is 3.7 µm. Using this value for the size of an Airy disc and a value of 0.565 µm for the wavelength of visible light, the size of a diffraction-limited aperture, *DLA*, can be estimated as

$$DLA = \frac{3.72}{1.22 \times 0.565} = 5.4$$

(Larmore, 1965; Born and Wolf, 1999; Padley, 2005; Johnson, 2010; Rista, 2012). This means that spatial resolution will be limited by diffraction when apertures smaller than the standard size of f/5.6 are used for recording images. Using the procedure outlined in (Larmore, 1965; Johnson, 2010; Rista, 2012), the spatial resolution values associated with the standard aperture settings of f/5.6 and f/16 were estimated as 5.3 µm and 11.6 µm, respectively. The 11.6 µm value for f/16 agrees well with the 9 µm determined by applying the ISO 12233 procedure. More importantly, the spatial resolution estimates indicate that an improvement of near 40% may be possible by increasing the aperture from f/16 to f/5.6 during image recording. A disadvantage of this, however, is that depth of field at f/5.6 is 2.5 times smaller than it is at f/16. For example, for UMNH VP 25852 this would be equivalent to recording, processing, and storing approximately 1,680 additional image files. Whether the increase in spatial resolution associated with apertures larger than f/16 is justified by an increase in perceived sharpness will depend on the relative importance of individual specimens.

A final point related to the photography is that the effect of focus stacking on the process of calibrating the camera and lens information in Photoscan is unknown. Metadata tags, defined by the Exif standard, were preserved through the focus-stacking procedure in the Helicon Focus software. This means that information preserved in the focus-stacked images included the camera make and model, lens make and

model, lens focal length, and various exposure settings including the image orientation, aperture, shutter speed, focal length, metering mode, and ISO speed. As shown in Table 1, lens calibration parameters were calculated by Photoscan for the focus-stacked images during the model optimization process. However, because focus stacking produces a composite image, it is possible that artifacts or errors introduced by the process occur in the composites. It will be important to address this issue in future work because the accuracy of the photogrammetry models produced in Photoscan depend critically on the quality of and metadata attached to the input images (Matthews, 2008; Matthews et al., 2016).

Lastly, another valuable feature of photogrammetry and the Agisoft Photoscan software in particular is that it can be used to export 3D models in stereo lithography file formats that are compatible with 3D printing. This was done for specimen UMNH VP 25852 and the solid model, shown in Figure 10, was produced using an on-line printing service (http://www.shapeways.com/). It has a total height of 100 mm or around 10 times that of the

Figure 10: Comparison of a 3D-printed model of specimen UMNH VP 25852, scaled up to a total height of 100 mm, compared to the actual specimen.

actual tooth which is also shown in Figure 10 for comparison. The shape, proportions, major details like the flutes, and even some finer-scale details of the actual tooth are preserved in the 3D-printed shape. The finest surface details of the tooth were not reproduced as well, but this is a limitation of the printing process rather than the digital model.

Geological setting and Taxonomic considerations

The region where these teeth were collected is in the north central of the USGS 7.5' Topographic of Washington Dome, Utah Quadrangle. The specific locality designation, according to the Utah Geological Survey database of paleontological sites, is W42s538.

The excavations that revealed the fossils were part of construction activities for the Southern Parkway Project, Washington County, Utah, USA. The W42s538 locality is along the southeast limb of the Virgin Anticline which has been extensively exposed by erosion (Biek et al., 2009). The roadway cuts through outcrops of the Lower Jurassic Kayenta Formation. In southwest Utah, the lower part of the Silty Facies dominates these outcrops which date to about 195-193 mya. The Silty Facies are considered fluvial and lacustrine deposits (Blakey, 1994; Milner and Spears, 2007) particularly in their lower strata (Milner et al., 2012) suggesting that the region may once have been characterized by the existence of large shallow lakes. Systematic excavations of the site before and during highway construction revealed an abundance of identifiable plant fossils (cycads, ferns, and horsetails), invertebrates (conchostracans, ostracods, and rare gastropods and bivalves), fishes (semionotids and palaeoniscoids), vertebrate tracks and traces (*Grallator*, *Eubrontes*, *Anomoepus*, *Kayentapus*, *Characichnos*, and *Unichna*), abundant vertebrate teeth, fish coprolites, and unidentifiable bone clasts. Of the vertebrate teeth, a high diversity of morphotypes are recognized including small and medium-sized theropods, ornithischians, a variety of unknown archosaurs, possible pterosaur, crocodylians, and fishes. Over 2,000 specimens were collected. These are housed at the Natural History Museum of Utah (UMNH), Salt Lake City, Utah, and at the St. George Dinosaur Discovery Site at Johnson Farm, St. George, Utah. Detailed descriptions of the various specimens are continuing.

The size and shape of specimen UMNH VP 25852 is similar to a deeply-fluted one associated with a temnospondyl amphibian, shown as Figure 9.54 in (Kay and Padian, 1994). However, the lack of in-folding of the flutes preclude this. Examining this tooth from its apex with the aid of the PDF model confirms that a symmetrical D-shape approximates its cross-sectional shape (Smith and Dodson, 2003) with the labial surface more prominently convex that the lingual surface. This also confirms the interpretation of orientation that was suggested earlier and further supports that a resorption pit may exist on the lingual side of the tooth. Teeth of this shape with virtually no recurvatures suggest possible association with a theropod dinosaur (Hendrickx et al., 2015).

Specimen UMNH VP 25853 has characteristics that tend to refer it to an ornithischian dinosaur, including (1) spatulate, triangular crown in both the labial or lingual views; (2) a well-developed neck between its crown and the location of root attachment; and, (3) evidence of prominent, relatively large denticles on both its mesial and distal edges (Sereno, 1991). It is tempting to associate the tooth with *Scutellosaurus lawleri* which is known from the Kayenta Formation in southwest North American (Colbert, 1981), and which could have teeth of similar size. On the other hand, it seems that some of these same features are widespread among archosauromorphs and they have evolved independently multiple times (Flynn et al., 2010). Teeth of similar shapes, for instance, also occur in heterodont crocodilians (Ősi, 2014). Ultimately, confident referral to specific taxa will require that both this tooth and specimen UMNH VP 25852 are better associated with skeletal remains.

SUMMARY

A macrophotography technique coupled with focus stacking was used to produce source images for photogrammetry of two isolated fossil teeth from the Lower Jurassic Kayenta Formation of southwest Utah. Focus stacking with Helicon Focus 6 software was used to produce completely focused images for input to Agisoft Photoscan photogrammetry software. The scaled three-dimensional representations created by photogrammetry are available at https://figshare.com/s/d205f5bee8cb2767f902 for specimen UMNH VP 25852 and

https://figshare.com/s/af8b4e74db21606a91bd, for specimen UMNH VP 25853. Judging by appearances, retention in the three-dimensional models of shape and surface details from the two-dimensional input images was excellent. These files can be used to examine, share, and store information about the teeth outside of the photogrammetry software. A stereo lithography file was also exported for UMNH VP 25852 model, and it was used to produce a 3D-printed model of this tooth.

Regarding the teeth, specimen UMNH VP 25852 has features associated with small theropod dinosaurs. Specimen UMNH VP 25853 has features associated with ornithischian dinosaurs. However, without reference to skeletal remains neither tooth could be unambiguously associated with a specific taxon.

ACKNOWLEDGMENTS

The Natural History Museum of Utah, Salt Lake City, Utah, allowed us to study these specimens. We thank Fred Overkamp and Scott Madsen for specimen preparation. Michael Duvall, Richard McCrea, Tommy Noble and especially Samantha Porter provided valuable assistance about photogrammetry technique and analysis. Brent Breithaupt and Elizabeth Freeman-Fowler provided many helpful comments for improving the manuscript. Neffra Matthews and Verónica Díez provided comprehensive and thoughtful formal reviews. This work was completed without the financial support of any institution or funding agency. The generous support of Agisoft LLC, St. Petersburg, Russia is greatly appreciated.

We also thank the Curry Fund of the Geologist's Association, which covered the costs of the article production.

REFERENCES CITED

Biek, R. F., P. D. Rowley, J. M. Hayden, D. B. Hacker, G. C. Willis, L. F. Hintze, R. E. Anderson, and K. D. Brown (eds.). 2009. Geologic Map of the St. George and East Part of the Clover Mountains 30'x60' Quadrangles, Utah Geological Survey Map 242, Washington and Iron Counties, Utah. Utah Geological Survey, Salt Lake City, Utah, USA.

Blakey, R.C. 1994. Paleogeographic and tectonic controls on some Lower and Middle Jurassic erg deposits, Colorado Plateau, p. 273-298. In J.A. Peterson, M.V. Caputo, and K.J. Franczyk (eds), Mesozoic systems of the Rocky Mountain Region, USA. Denver: Rocky Mountain Section of the Society of Economic Paleontologists and Mineralogists.

Born, M., and E. Wolf. 1999. Principles of Optics, 7th Ed. Cambridge University Press, New York, USA, 952 pp.

Breithaupt, B. H., N. A. Matthews, and T. A. Noble. 2004. An integrated approach to three-dimensional data collection at dinosaur tracksites in the Rocky Mountain West. Ichnos 11:11–26.

Flynn, J. J., S. J. Nesbitt, J. M. Parrish, L. Ranivoharimanana, and A. R. Wyss. 2010. A new species of *Azendohsaurus* (Diapsida: Archosauromorpha) from the Triassic Isalo Group of southwestern Madagascar: cranium and mandible. Palaeontology 53:669–688.

Cognysis-Inc.com. 2016. Stackshot 3X – Using the Virtual Object Kit. (Internet, most recent access: January, 2017) Available from: https://www.cognisys-inc.com/how-to/stackshot3x/virtual-objects.php.

Colbert, E. H. 1981. A primitive ornithischian dinosaur from the Kayenta Formation of Arizona. Museum of Northern Arizona Press 53:1-61.

Falkingham, P. L. 2012. Acquisition of high resolution 3D models using free, open-source, photogrammetric software, Palaeontologia Electronica 15(1):15.

Hendrickx, C., O. Mateus, and R. Araújo. 2015. A proposed terminology of theropod teeth (Dinosauria, Saurischia), Journal of Vertebrate Paleontology, 35(5):e982797. doi: 10.1080/02724634.2015.982797

ISO 12233. 2000. Photography – Electronic still-picture cameras – Resolution measurements, First edition, 2000-09-01. Reference number ISO 12233:2000(E), International Organization for Standardization. 40 pp.

Johnson, C. S. 2010. Science for the Curious Photographer: An Introduction to the Science of Photography. A. K. Peters, Ltd., Natick, MA, USA, 200 pp.

Kay, F. T., and K. Padian. 1994. Microvertebrates from the Placerias Quarry: a window on Late Triassic vertebrate diversity in the American Southwest, pp. 171-196. In N. C. Fraser and H.-D. Sues (eds), In the Shadow of the Dinosaurs: Early Mesozoic Tetrapods. Cambridge University Press, Cambridge, UK.

Larmore, L. 1965. Introduction to Photographic Principles. 2nd ed. Dover Publications, Inc., New York, NY, USA, 229 pp.

Mallison, H., and O. Wings. 2014. Photogrammetry in paleontology – a practical guide. Journal of Paleontological Techniques 12:1-31.

Matthews, N. A. 2008. Aerial and Close-Range Photogrammetric Technology: Providing Resource Documentation, Interpretation, and Preservation. Technical Note 428. U.S. Department of Interior, Bureau of Land Management, National Operations Center, Denver, Colorado, USA, 42 pp.

Matthews, N. A., T. A. Noble, and B. H. Breithaupt. 2016. Close-range photo-grammetry for 3D ichnology: the basics of photogrammetric ichnology; pp. 28–55 in P. L. Falkingham, D. Marty, and M. Richter (eds.), Dinosaur Tracks: The Next Steps. Indiana University Press, Bloomington, Indiana, USA.

Milner, A. R. C., and S. Z. Spears. 2007. Mesozoic and cenozoic ichnology of southwestern Utah; pp. 1-85 In W. R. Lund (ed.), Field Guide to Geologic Excursions in Southern Utah, Geological Society of America, Rocky Mountain Section 2007 Annual Meeting, St. George, Utah. Utah Geological Association Publication 35, Utah Geological Association, Salt Lake City, Utah, USA. Available from: http://www.utahgeology.org/pub35_su_guide/UGA35.pdf.

Miln e , A. R. C., T. A. Birthisel, J. I. Kirkland, B. H. Breithaupt, N. A. Matthews, M. G. Lockley, V. L. Santucci, S. Z. Gibson, D. D. DeBlieux, M. Hurlburt, J. D. Harris, and P. E. Olsen. 2012. Tracking Early Jurassic dinosaurs across southwestern Utah and the Triassic–Jurassic transition. Field Trip Guide Book for the 71st Annual Meeting of the Society of Vertebrate Paleontology: Nevada State Museum Paleontological Papers 1:1–107.

Minnesota Anthropology. Creating Artifact Models in Agisoft Photoscan. Available from: https://www.youtube.com/watch?v=qKWjPNlRK_I&list=PLZzVwXTSDAJ238A0AJJIIxr9wKV9nioO5 (January, 2017).

Nguyen, C. V., D. R. Lovell, M. Adcock, and J. La Salle. 2014. Capturing natural-colour 3D models of insects for species discovery and diagnostics. PLoS One 9:e94346.

Ősi, A. 2014. The evolution of jaw mechanism and dental function in heterodont crocodyliforms, Historical Biology 26(3):279-414. doi:10.1080/08912963.2013.777533

Padley, P. 2005. Diffraction from a Circular Aperture. OpenStax CNX. Available from: http://cnx.org/contents/586c6da1-e147-42be-87af-9925e4070808@1 (January, 2017).

Porter, S. T., M. Roussel, and M. Soressi. 2016. A simple photogrammetry rig for the reliable creation of 3D artifact models in the field lithic examples from the early upper Paleolithic sequence of Les Cottés (France). Advances in Archaeological Practice 4:71–86. doi:https://doi.org/10.7183/2326-3768.4.1.71

Rista, J. 2012. Photography Community Blog. Stack Exchange: Jonathan Rista. Available from: http://photo.blogoverflow.com/2012/06/the-realities-of-resolution/ (January, 2017).

Sereno, P. C. 1991. *Lesothosaurus*, "Fabrosaurids," and the Early Evolution of Ornithischia. Journal of Vertebrate Paleontology 11(2):168-197. doi:10.1080/02724634.1991.10011386

Smith, J. B., and P. Dodson. 2003. A proposal for a standard terminology of anatomical notation and orientation in fossil vertebrate dentitions. Journal of Vertebrate Paleontology 23:1–12.

USA.Canon.com, eos. eos-rebelt6s-760d-im2-en.pdf. Available from: https://www.usa.canon.com/internet/portal/us/home/support/details/cameras/dslr/eos-rebel-t6s-ef-s-18-135mm-is-stm-lens-kit?tab=manuals (January, 2017).

USA.Canon.com, mpe. mpe65f28-1-5x-im2-eng.pdf. Available from: https://www.usa.canon.com/internet/portal/us/home/support/details/lenses/ef/macro/mp-e-65mm-f-2-8-1-5x-macro-photo (January, 2017)

Additional images and material can be downloaded at http://www.jpaleontologicaltechniques.org/